Nanoscale Advances

ROYAL SOCIETY OF CHEMISTRY

PAPER

View Article Online
View Journal | View Issue

Check for updates

Cite this: *Nanoscale Adv.*, 2025, **7**, 1552

Magnetic resorcinol–formaldehyde supported isatin-Schiff-base/Fe as a green and reusable nanocatalyst for the synthesis of pyrano[2,3-*d*] pyrimidines

Fatemeh Kiani, Dawood Elhamifar * and Shiva Kargar

Received 17th September 2024
Accepted 21st December 2024

DOI: 10.1039/d4na00775a

rsc.li/nanoscale-advances

Herein, a novel magnetic resorcinol–formaldehyde-supported isatin-Schiff-base/Fe complex (Fe_3O_4@RF-ISB/Fe) is prepared and characterized and its catalytic performance is investigated in the synthesis of pyrano[2,3-*d*]pyrimidines. The Fe_3O_4@RF-ISB nanomaterial was prepared through the chemical immobilization of (3-aminopropyl)trimethoxysilane over the Fe_3O_4@RF composite, followed by treatment with isatin. The Fe_3O_4@RF-ISB was then reacted with $FeCl_3{\cdot}6H_2O$ to afford the Fe_3O_4@RF-ISB/Fe nanocatalyst. Characterization through FT-IR, EDX, PXRD, VSM, SEM and ICP techniques confirmed that the magnetite surface was successfully modified with RF/ISB-Fe while preserving its crystalline structure. The SEM image revealed spherical particles with an average size of 44 nm for the designed nanocomposite. Various aromatic aldehydes were used as substrates in the presence of 0.01 g of Fe_3O_4@RF-ISB/Fe to give the corresponding pyranopyrimidines in high yields (88–95%) within short reaction times (30–55 minutes) at RT. The designed magnetic catalyst maintained its activity for nine runs.

Open Access Article. Published on 20 January 2025. Downloaded on 2/7/2026 7:36:55 PM.
This article is licensed under a Creative Commons Attribution-NonCommercial 3.0 Unported Licence.

1. Introduction

Magnetic nanocomposites play a vital role in numerous fields, such as catalysis, drug delivery, energy harvesting, plasmonics, and magnetic resonance imaging (MRI).[1–6] In these nanocomposites, the high chemical reactivity of magnetic nanoparticles (MNPs) can be effectively controlled by a chemically inert shell which may consist of materials such as silica, alumina, polymers, or carbon. Recent developments in this area include Mag@mSiO_2/IL-Cu,[7] Fe_3O_4@C–TiO_2–Ag,[8] Fe_3O_4@-SiO_2@La_2O_3,[9] $Mo_{72}V_{30}$@Fe_3O_4/C[10] and Fe_3O_4/ZIF-8/TiO_2.[11] Among the different types of shells, resorcinol–formaldehyde (RF) resin has gained significant interest due to its distinctive properties. These include a hydrophobic inner framework, a surface rich in phenolic hydroxyl groups that facilitates the accumulation of reactants near the catalytic active sites, and advantages such as high biocompatibility, non-toxicity, and cost-effectiveness.[12–16] Therefore, coating magnetic nanoparticles with an RF shell not only enhances their chemical stability and prevents aggregation but also utilizes the distinctive hydrophobic and biocompatible properties of RF, thereby making these nanocomposites particularly effective for catalytic applications.

Meanwhile, Schiff-base ligands have garnered significant attention in the chemical and materials sciences due to their efficient complexation with a wide variety of transition metal ions, excellent solubility, and superior catalytic performance. Furthermore, Schiff-base ligands are used to improve catalytic efficiency by linking the catalytic centers to solid supports.[17–23] Recent studies in this area include reports such as Fe_3O_4@-BOS@SB/In,[24] Cu/SB–Fe_3O_4,[25] and $[M^{II}(L)(Cl)(H_2O)_2]{\cdot}H_2O$,[26] BPMO@ISB/Mn(II).[27]

Recently, multicomponent reactions (MCRs) owing to their simple operation, atom economy and high efficiency, have become a crucial tool in organic synthesis and medicinal chemistry, attracting significant attention from chemists.[28,29] Pyrano[2,3-*d*]pyrimidines, prepared through multicomponent reactions, exhibit notable biological activities, including anticancer, antispasmodic, antianaphylactic, and anticoagulant properties. Therefore, the advancement of methods for their effective synthesis remains a highly significant area among chemists. Despite the establishment of various methods for synthesizing pyrano[2,3-*d*]pyrimidines, these techniques have significant limitations, such as high catalyst loadings, low yields, the use of expensive ligands, complex work-ups, difficulties in separating products from catalysts, and the use of hazardous solvents.[30–32] Hence, there is a critical need for the development of a more environmentally friendly, efficient, straightforward, and cost-effective method for synthesizing pyrano[2,3-*d*]pyrimidines.

Considering all these aspects, in this work, a novel, and environmentally friendly magnetic nanocatalyst supported isatin Schiff-base/Fe complex, denoted as Fe_3O_4@RF-ISB/Fe, is

Department of Chemistry, Yasouj University, Yasouj, 75918-74831, Iran. E-mail: d.elhamifar@yu.ac.ir

© 2025 The Author(s). Published by the Royal Society of Chemistry

Open Access Article. Published on 20 January 2025. Downloaded on 2/7/2026 7:36:55 PM.
This article is licensed under a Creative Commons Attribution-NonCommercial 3.0 Unported Licence.

prepared, characterized and applied as a effective catalyst for the green synthesis of pyrano[2,3-*d*]pyrimidines.

2. Experimental section

2.1 Synthesis of Fe_3O_4@RF

Initially, Fe_3O_4 nanoparticles (NPs) were synthesized using a method described in our previous work.[33] After that, 150 mL of deionised (DI) water was used to disperse the 1 g of Fe_3O_4 NPs. Following 10 minutes of ultrasonic treatment, ammonia (0.3 mL, 25 wt%) and resorcinol (0.4 g) were introduced into the solution, which was then was agitated at 30 °C for 1 hour. Following a dropwise addition of 0.6 mL of formaldehyde, the mixture was constantly stirred for 6 hours. After that, the mixture was heated for five hours at 80 °C to complete the procedure. After collecting the magnetic material, it was thoroughly rinsed with EtOH and deionized (DI) water and dried at 70 °C for 6 h.[34]

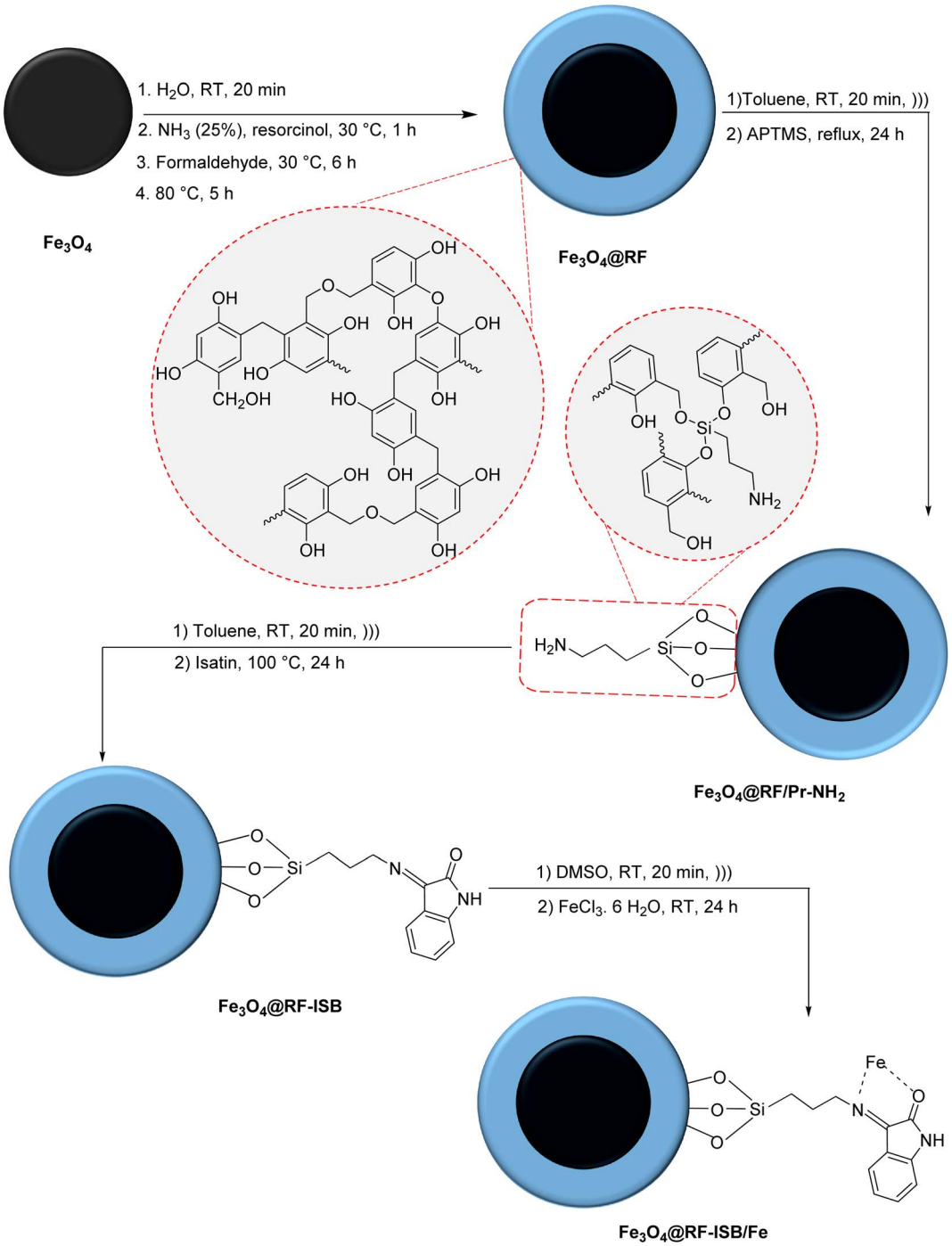

Scheme 1 Preparation of the Fe_3O_4@RF-ISB/Fe nanocatalyst.

Open Access Article. Published on 20 January 2025. Downloaded on 2/7/2026 7:36:55 PM. This article is licensed under a Creative Commons Attribution-NonCommercial 3.0 Unported Licence.

2.2 Synthesis of Fe_3O_4@RF/Pr-NH_2

To achieve this, 1 g of Fe_3O_4@RF nanoparticles was dispersed in 25 mL of toluene at 25 °C for 20 minutes. After adding 0.26 g of (3-aminopropyl)trimethoxysilane (APTMS), the mixture was refluxed at 100 °C for 24 hours. The resulting magnetic material was subsequently collected, rinsed with ethanol and DI water, and dried at 70 °C for 6 hours.

2.3 Synthesis of Fe_3O_4@RF-ISB

For this, 1 g of Fe_3O_4@RF/Pr-NH_2 was fully dispersed in 20 mL of toluene for 20 minutes. Subsequently, 0.6 g of isatin was introduced into the reaction vessel, and the mixture was agitated and refluxed for 24 hours. The resulting product was further subjected to magnetic separation, rinsed with ethanol and DI water, and dried in an oven at 60 °C for 12 hours.

2.4 Synthesis of Fe_3O_4@RF-ISB/Fe

Initially, 1 g of Fe_3O_4@RF-ISB was fully dispersed in 20 mL of DMSO for 20 minutes. Then, the reaction vessel was agitated at room temperature for 24 hours after adding 0.2 g of $FeCl_3 \cdot 6H_2O$. After being separated using a magnet, the final product was washed with ethanol and DI water and then dried for 12 hours at 60 °C. The ICP analysis was performed on both Fe_3O_4@RF-ISB and Fe_3O_4@RF-ISB/Fe. The results indicated that the Fe loading onto the material framework was 0.14 mmol Fe per g.

2.5 Procedure for the synthesis of pyrano[2,3-*d*]pyrimidines using the Fe_3O_4@RF-ISB/Fe nanocatalyst

To carry out the reaction, aldehyde (1 mmol), malononitrile (1 mmol), barbituric acid (1 mmol), and 0.01 g of Fe_3O_4@RF-ISB/Fe were added to a reaction vessel containing EtOH (10 mL) and stirred at RT. Upon completion, monitored by TLC, the Fe_3O_4@RF-ISB/Fe catalyst was removed using an external magnet. The pure products were obtained by recrystallization from EtOH.

3. Results and discussion

3.1 Characterization of Fe_3O_4@RF-ISB/Fe

Scheme 1 illustrates the synthesis pathway for the Fe_3O_4@RF-ISB/Fe nanocomposite. Initially, Fe_3O_4@RF NPs were synthesized *via* the interface polymerization of resorcinol and formaldehyde on Fe_3O_4 NPs under alkaline conditions. The RF shell was then chemically modified with (3-aminopropyl)trimethoxysilane (APTMS), resulting in Fe_3O_4@RF/Pr-NH_2. This nanomaterial was subsequently reacted with isatin to afford Fe_3O_4@RF-ISB. Finally, the Fe_3O_4@RF-ISB support was treated with $FeCl_3 \cdot 6H_2O$ to yield the Fe_3O_4@RF-ISB/Fe nanocomposite.

Fig. 1 displays the FTIR spectra of the synthesized materials, including Fe_3O_4@RF (a), Fe_3O_4@RF/Pr-NH_2 (b), Fe_3O_4@RF-ISB (c), and Fe_3O_4@RF-ISB/Fe (d). For all samples, the FTIR analysis revealed a characteristic absorption peak for the Fe–O bond at 588 cm^{-1} and a stretching vibration of the O–H bond at 3419 cm^{-1}. The absorption bonds appeared at 2857–2932 and

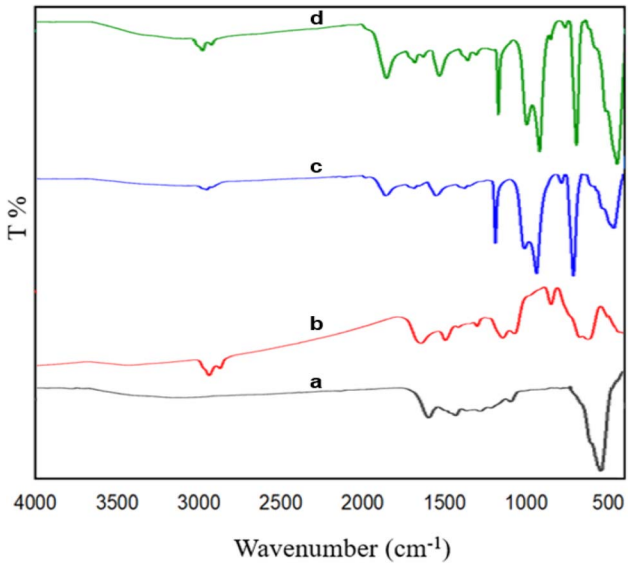

Fig. 1 The FTIR spectra of Fe_3O_4@RF (a), Fe_3O_4@RF/Pr-NH_2 (b), Fe_3O_4@RF-ISB (c), and Fe_3O_4@RF-ISB/Fe (d).

1450 cm^{-1}, corresponding to the aliphatic C–H stretching and bending vibrations of the propyl amines and RF resin, respectively. Additionally, the signals at 1021 and 1110 cm^{-1} are attributed to the C–O–C methylene ether bridges between resorcinol units.[35,36] The presence of the Si–O–Si signals at 806 and 1029 cm^{-1} supported the successful surface modification of Fe_3O_4@RF with (3-aminopropyl)trimethoxysilane (Fig. 1b–d). Furthermore, the peak at 1621 cm^{-1} is attributed to the C=N bond, indicating that the isatin-Schiff-base (ISB) ligand was successfully formed on the material surface (Fig. 1c and d).[37]

Powder X-ray diffraction (PXRD) analysis was conducted to examine the crystallinity of the Fe_3O_4@RF-ISB/Fe nanocomposite. As shown in Fig. 2, the wide-angle PXRD pattern reveals six peaks at 2θ values of 30.4°, 35.82°, 43.03°, 54.22°, 57.36°, and 62.98°, corresponding to the (220), (311), (400), (422), (511), and (440) crystal planes, respectively. These observations are consistent with the PXRD pattern of Fe_3O_4,

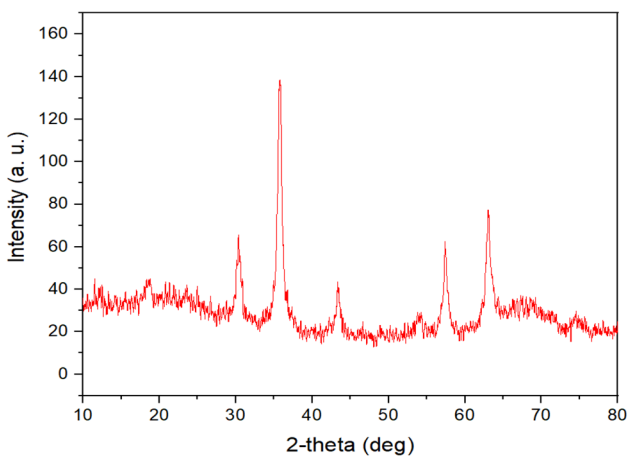

Fig. 2 The PXRD pattern of the Fe_3O_4@RF-ISB/Fe.

© 2025 The Author(s). Published by the Royal Society of Chemistry

Open Access Article. Published on 20 January 2025. Downloaded on 2/7/2026 7:36:55 PM.
This article is licensed under a Creative Commons Attribution-NonCommercial 3.0 Unported Licence.

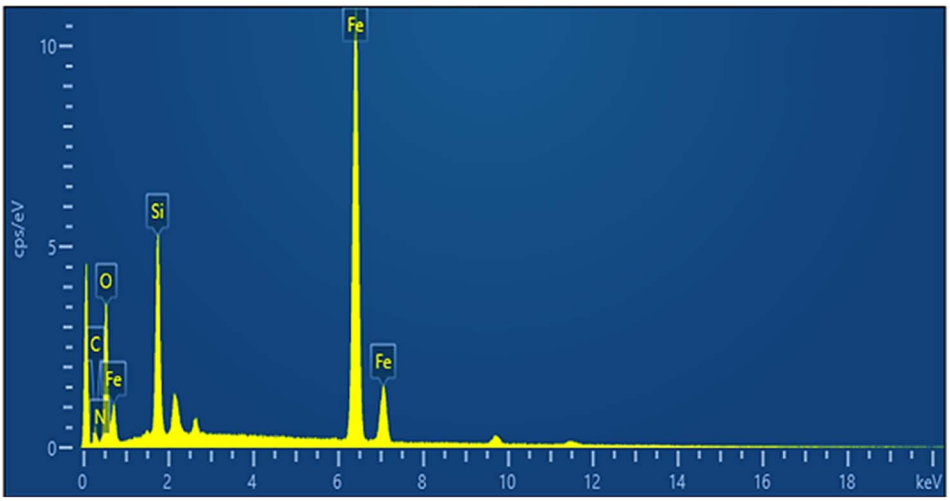

Fig. 3 The EDX spectrum of Fe_3O_4@RF-ISB/Fe.

indicating that these NPs retain high stability throughout the modification processes.[38,39]

Fig. 3 shows the EDX spectrum of the Fe_3O_4@RF-ISB/Fe catalyst. The EDX spectrum confirms the presence of C, N, O, Si, and Fe in the sample. This result is in accordance with the FTIR analysis, confirming the effective incorporation and immobilization of the expected species in the Fe_3O_4@RF-ISB/Fe nanocomposite.

The magnetic properties of Fe_3O_4@RF and Fe_3O_4@RF-ISB/Fe nanomaterials were investigated using a vibrating sample magnetometer (VSM, Fig. 4). The saturation magnetization values obtained were 50 and 39.8 emu g^{-1}, respectively, for Fe_3O_4@RF and Fe_3O_4@RF-ISB/Fe. The observed decrease in magnetic properties after modification is attributed to the successful immobilization of the isatin-Schiff-base/Fe complex on the Fe_3O_4@RF NPs.

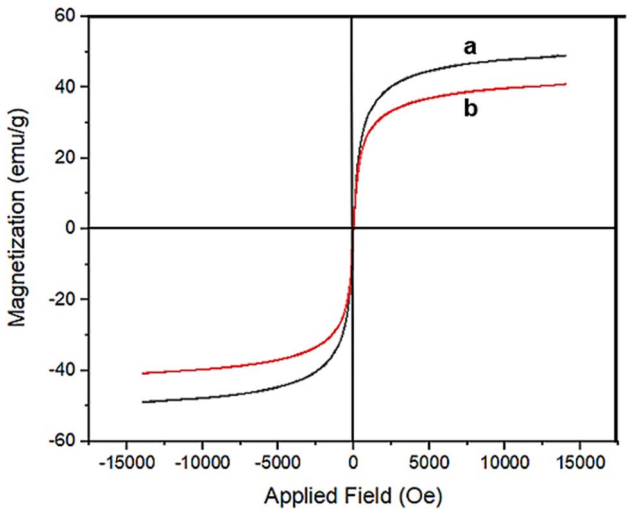

Fig. 4 The VSM diagrams of Fe_3O_4@RF (a) and Fe_3O_4@RF-ISB/Fe (b) nanocomposites.

The SEM analysis was conducted to examine the morphology of the Fe_3O_4@RF-ISB/Fe nanocomposite (Fig. 5). The analysis revealed that the catalyst exhibits a spherical morphology with an average particle size of approximately 44 nm.

3.2 Catalytic activity of the Fe_3O_4@RF-ISB/Fe nanocomposite

After characterization, the performance of the Fe_3O_4@RF-ISB/Fe catalyst was investigated in the synthesis of pyrano[2,3-*d*] pyrimidines. The condensation between barbituric acid, benzaldehyde and malononitrile at room temperature (RT) was selected as a test model to optimize the reaction conditions. By evaluating the effect of several parameters, such as catalyst amount and solvent, the optimal conditions were determined (Table 1). Initially, the effect of solvent-free conditions, as well as the use of H_2O and EtOH solvents, was investigated (Table 1, entries 1–3). The results demonstrated that the highest yield of 95% was observed with EtOH (Table 1, entry 3). The reaction progress was also affected by the amount of catalyst, and 0.01 g of Fe_3O_4@RF-ISB/Fe provided the best result (Table 1, entry 3). Interestingly, there was no noticeable difference in the product yield when the catalyst amount increased to 0.015 g (Table 1, entry 5). It should be noted that no product was observed in the absence of the catalyst (Table 1, entry 6). To demonstrate the role of supported-Fe centers in the catalytic process, the reaction was performed in the presence of Fe-free Fe_3O_4@RF and Fe_3O_4@RF-ISB materials under identical reaction conditions (Table 1, entries 7 and 8). Interestingly, only a low yield of the desired product was obtained in the latter cases. These findings indicate that the supported-Fe species play a major role in catalyzing the reaction. In addition, the catalytic activity of Fe_3O_4@RF-ISB/Fe was compared with that of $FeCl_3 \cdot 6H_2O$ salt (Table 1, entry 3 *vs.* entry 9). The result indicates that the reaction achieves a satisfactory conversion using $FeCl_3 \cdot 6H_2O$. This result confirms that the catalytic activity of Fe_3O_4@RF-ISB/Fe is comparable to that of the homogeneous $FeCl_3 \cdot 6H_2O$ catalyst, as both systems achieve similar yields. This finding

© 2025 The Author(s). Published by the Royal Society of Chemistry

Open Access Article. Published on 20 January 2025. Downloaded on 2/7/2026 7:36:55 PM.
This article is licensed under a Creative Commons Attribution-NonCommercial 3.0 Unported Licence.

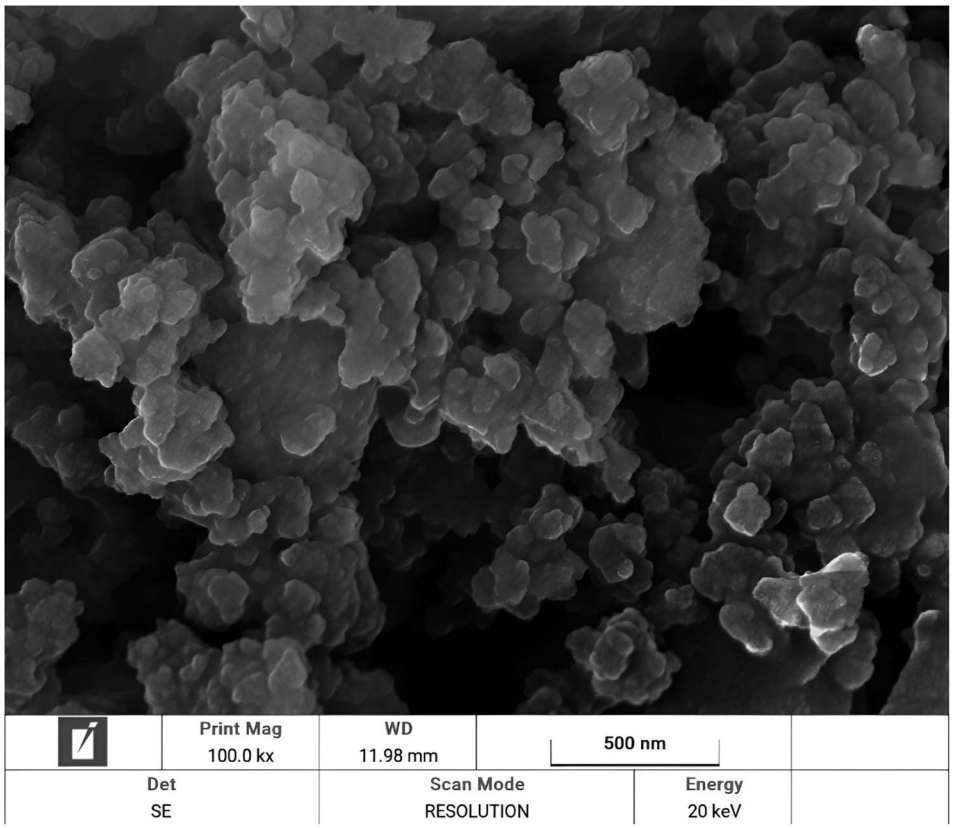

Fig. 5 The SEM image of the Fe_3O_4@RF-ISB/Fe nanocomposite.

Table 1 Effect of different parameters in the synthesis of pyranopyrimidines

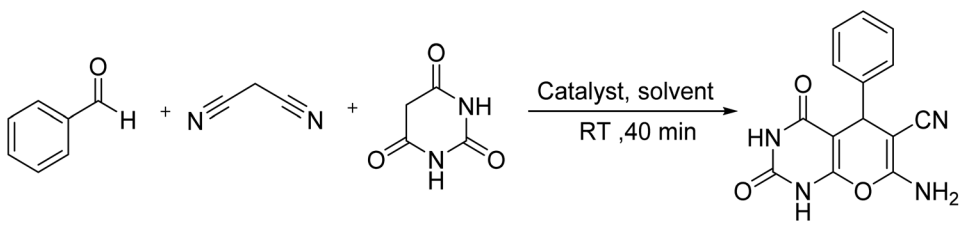

Entry	Solvent	Catalyst	Catalyst loading (g)	Yield (%)
1	—	Fe_3O_4@RF-ISB/Fe	0.01	86
2	H_2O	Fe_3O_4@RF-ISB/Fe	0.01	76
3	**EtOH**	**Fe_3O_4@RF-ISB/Fe**	**0.01**	**95**
4	EtOH	Fe_3O_4@RF-ISB/Fe	0.005	75
5	EtOH	Fe_3O_4@RF-ISB/Fe	0.015	96
6	EtOH	—	—	—
7	EtOH	Fe_3O_4@RF	0.01	15
8	EtOH	Fe_3O_4@RF-ISB	0.01	14
9	EtOH	$FeCl_3 \cdot 6H_2O$	0.004	96

clearly demonstrates that the supported Fe(III) species exhibit high efficiency, closely resembling the catalytic behavior of free Fe(III) ions, while also providing significant advantages in terms of recoverability and reusability. Accordingly, the following optimal parameters were chosen: room temperature, EtOH as the solvent, and 0.01 g of the Fe_3O_4@RF-ISB/Fe catalyst.

Following condition optimization (Table 1, entry 3), various aldehyde derivatives were employed as substrates. As illustrated in Table 2, the corresponding pyranopyrimidines were formed

 © 2025 The Author(s). Published by the Royal Society of Chemistry

Open Access Article. Published on 20 January 2025. Downloaded on 2/7/2026 7:36:55 PM. This article is licensed under a Creative Commons Attribution-NonCommercial 3.0 Unported Licence.

Table 2 Synthesis of pyranopyrimidines using Fe_3O_4@RF-ISB/Fe

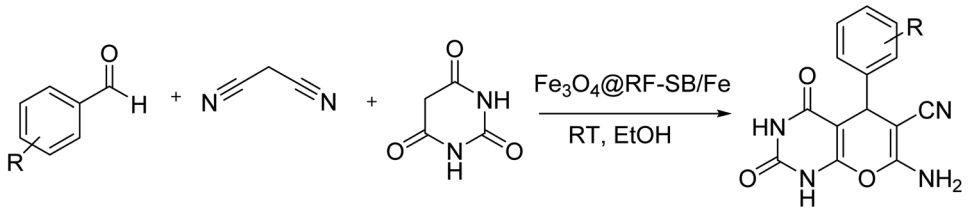

Entry	Aldehyde	Time (min)	Yield (%)	Mp found (°C)	Mp reported (°C)
1	PhCHO	40	95	219–221	222–224 (ref. 40)
2	4-Cl–PhCHO	35	91	240–242	242–244 (ref. 41)
3	4-Me–PhCHO	50	88	227–229	226–227 (ref. 42)
4	4-MeO–PhCHO	55	90	268–270	268–271 (ref. 40)
5	3-NO_2–PhCHO	35	94	265–267	265 (ref. 41)
6	4-Br–PhCHO	30	93	230–232	235–236 (ref. 42)

in high yields from all types of aldehydes. The remarkable performance of the Fe_3O_4@RF-ISB/Fe catalyst in the synthesis of various derivatives of pharmacologically active pyranopyrimidines was confirmed by the fact that electronic characteristics and the substituent positions had a little effect on this process.

In the following investigation, the recoverability and reusability of the Fe_3O_4@RF-ISB/Fe catalyst were evaluated. After completing the reaction, the Fe_3O_4@RF-ISB/Fe catalyst was magnetically separated and reused under the same conditions as the initial run. The results indicated that the Fe_3O_4@RF-ISB/Fe catalyst retained its effectiveness for at least nine cycles, highlighting its remarkable durability under the optimized conditions (Fig. 6).

A leaching test was performed to investigate the nature of the Fe_3O_4@RF-ISB/Fe catalyst under the applied conditions. During the test, the catalyst was removed from the reaction mixture after reaching a 50% conversion. The reaction of the residue was then allowed to continue for 60 min. The result demonstrated no significant increase in conversion, confirming the heterogeneous nature of the designed catalyst. Additionally, the ICP analysis proved the absence of Fe species in the reaction vessel confirming no leaching of the active Fe catalyst under the applied conditions. These results demonstrate the successful immobilization and high stability of the active Fe species, which is attributed to the Schiff-base ligand, preventing Fe-leaching during the reaction.

The PXRD analysis of the recovered Fe_3O_4@RF-ISB/Fe revealed six peaks at $2\theta = 30.48°$, 35.75°, 43.2°, 54.2°, 57.32°, and 63.05° (Fig. 7), which aligns well with the PXRD pattern of the fresh nanocatalyst. This confirms the exceptional stability of the crystalline structure of magnetite nanoparticles even after nine cycles of recovery and reuse.

A proposed mechanism for the synthesis of pyrano[3,2-*d*] pyrimidine derivatives catalyzed by Fe_3O_4@RF-ISB/Fe is presented in Scheme 2. The initial step involves forming intermediate **1** through a Knoevenagel condensation between malononitrile and the Fe-activated aldehyde. Subsequently, as

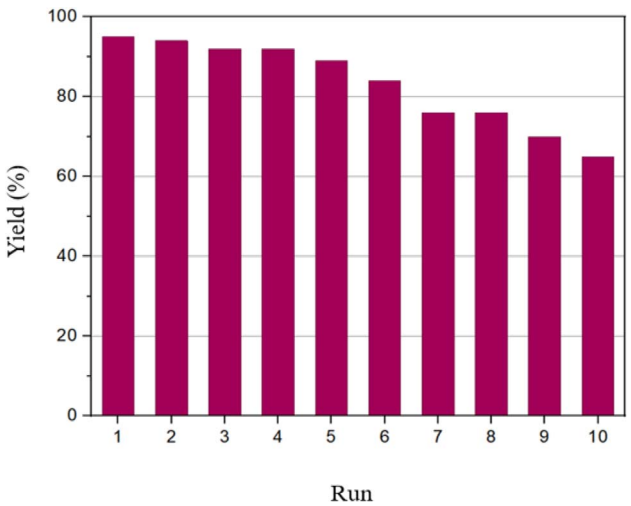

Fig. 6 Recoverability and reusability of the Fe_3O_4@RF-ISB/Fe nanocatalyst.

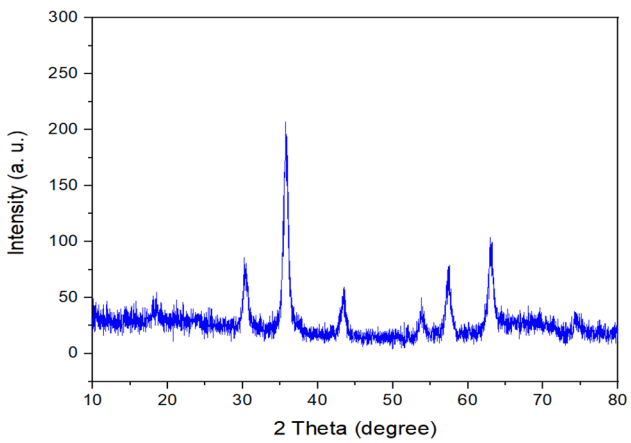

Fig. 7 The PXRD pattern of the recovered Fe_3O_4@RF-ISB/Fe nanocatalyst.

Open Access Article. Published on 20 January 2025. Downloaded on 2/7/2026 7:36:55 PM.
This article is licensed under a Creative Commons Attribution-NonCommercial 3.0 Unported Licence.

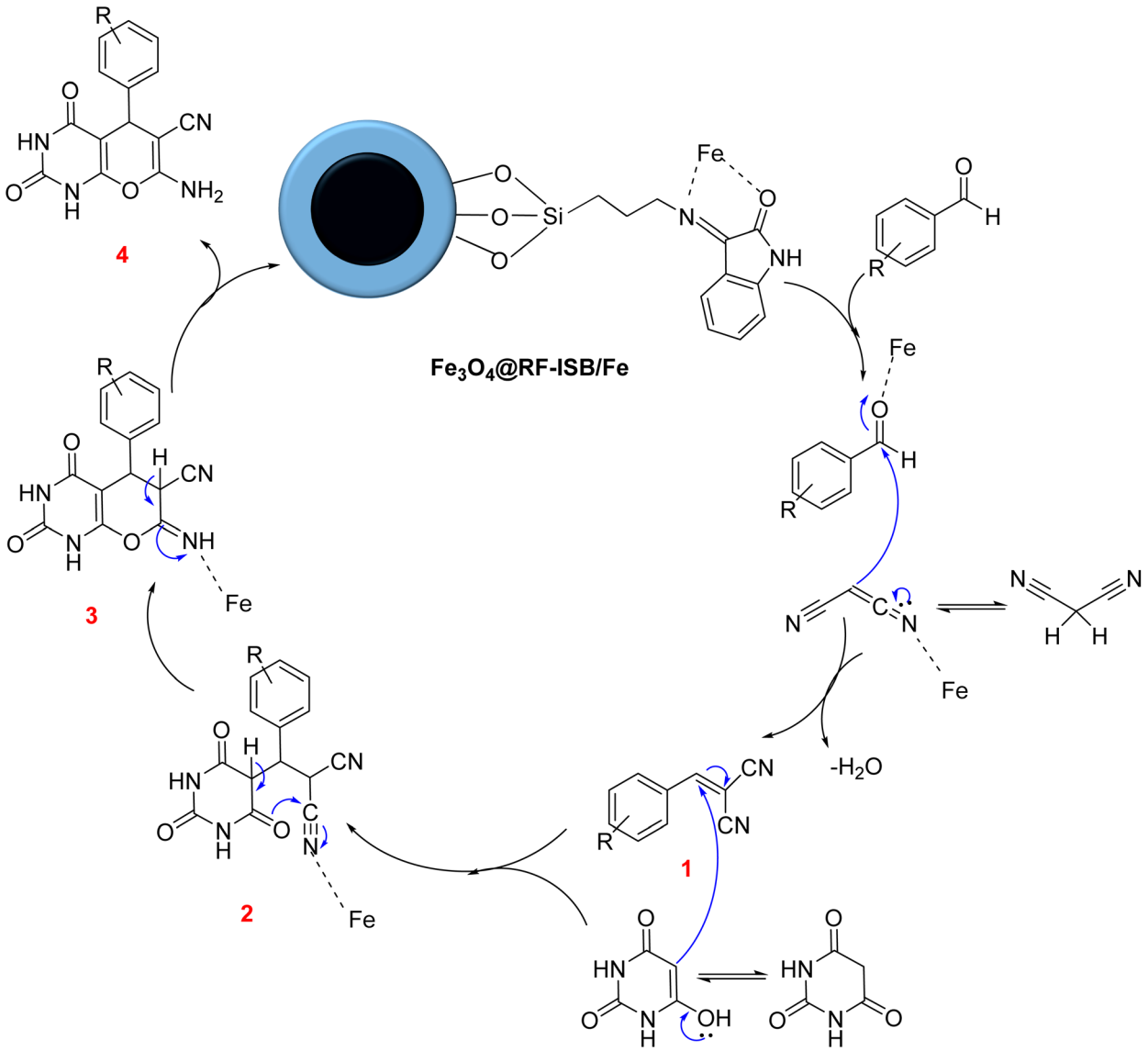

Scheme 2 A plausible mechanism for the synthesis of pyrano[2,3-*d*]pyrimidines using Fe_3O_4@RF-ISB/Fe.

Table 3 Comparative study of the efficiency of Fe_3O_4@RF-ISB/Fe with the former catalysts in the synthesis of pyrano[2,3-*d*]pyrimidines

Entry	Catalyst	Conditions	Time	Recovery times	Ref.
1	$[BMIm]BF_4$	Cat. (1.5 g), solvent-free, 90 °C	180 min	4	43
2	Fe_3O_4@cellulose	Cat. (5 mg), H_2O, 25 °C	35 min	5	30
3	L-Proline	Cat. (5 mol%), EtOH, 25 °C	40 min	—	43
4	Fe_3O_4@RF-ISB/Fe	Cat. (0.01 g), EtOH, 25 °C	40 min	9	This work

a Michael acceptor, this intermediate reacts with the enol form of barbituric acid to produce intermediate **2**. Next, intermediate **2** undergoes an intramolecular cyclization to form intermediate **3**. Finally, the desired product **4** is obtained through a tautomerization process.

The performance of the Fe_3O_4@RF-ISB/Fe catalyst was compared with that of various catalytic systems previously reported for the synthesis of pyrano[2,3-*d*]pyrimidines (Table 3). The study showed that the present catalyst outperforms previously reported catalytic systems in terms of mild reaction conditions, reaction rates, and recovery times.

4. Conclusion

In summary, a novel magnetic RF modified with an isatin-Schiff-base/Fe (Fe_3O_4@RF-ISB/Fe) complex was successfully

© 2025 The Author(s). Published by the Royal Society of Chemistry

Open Access Article. Published on 20 January 2025. Downloaded on 2/7/2026 7:36:55 PM. This article is licensed under a Creative Commons Attribution-NonCommercial 3.0 Unported Licence.

designed, prepared, characterized and applied as a powerful catalyst. The FT-IR and EDX analyses clearly indicated that the RF moieties were successfully coated/immobilized on the magnetic NPs. The PXRD analysis further confirmed that the crystalline structure of the Fe_3O_4 NPs remains highly stable throughout the modification process. Additionally, the SEM image of Fe_3O_4@RF-ISB/Fe revealed well-defined spherical particles of the nanomaterial. The Fe_3O_4@RF-ISB/Fe nanocomposite was effectively employed as a robust and highly recoverable catalyst for the synthesis of pyrano[2,3-*d*]pyrimidines, providing the desired products in high yields and short reaction times under mild conditions. Due to the advantages of the Fe_3O_4@RF-ISB/Fe nanocatalyst, including simple preparation, high stability, and ease of recovery and separation, this catalyst exhibits significant potential for use in various important organic reactions, such as other multicomponent processes, C–H activation, nucleophilic substitution of benzylic C–X bonds, C–N bond formation, and so on.

Data availability

All data and materials are included in the manuscript.

Conflicts of interest

There are no conflicts to declare.

Acknowledgements

The authors acknowledge Yasouj University and the Iran National Science Foundation (INSF) for supporting this work.

References

1 P. D. Tomke and V. K. Rathod, Facile fabrication of silver on magnetic nanocomposite (Fe_3O_4@chitosan–AgNP nanocomposite) for catalytic reduction of anthropogenic pollutant and agricultural pathogens, *Int. J. Biol. Macromol.*, 2020, **149**, 989–999.

2 Y. Huang, L.-c. Nengzi, X. Zhang, J. Gou, Y. Gao, G. Zhu, Q. Cheng and X. Cheng, Catalytic degradation of ciprofloxacin by magnetic CuS/Fe_2O_3/Mn_2O_3 nanocomposite activated peroxymonosulfate: influence factors, degradation pathways and reaction mechanism, *Chem. Eng. J.*, 2020, **388**, 124274.

3 M. Abd El-Aal, A. E.-A. A. Said, M. N. Goda, E. F. A. Zeid and S. M. Ibrahim, Fe_3O_4@CMC-Cu magnetic nanocomposite as an efficient catalyst for reduction of toxic pollutants in water, *J. Mol. Liq.*, 2023, **385**, 122317.

4 S. Naghash-Hamed, N. Arsalani and S. B. Mousavi, The catalytic performance of $CuFe_2O_4$@CQD nanocomposite as a high-perform heterogeneous nanocatalyst in nitroaniline group reduction, *Sci. Rep.*, 2023, **13**, 3329.

5 A. Adam and D. Mertz, Iron oxide@mesoporous silica core-shell nanoparticles as multimodal platforms for magnetic resonance imaging, magnetic hyperthermia, near-infrared light photothermia, and drug delivery, *Nanomaterials*, 2023, **13**, 1342.

6 A. F. Oliveira and E. M. B. de Sousa, Synthesis and characterization of MSN/Fe_3O_4/Gd_2O_3 nanocomposite as theranostic systems, *J. Nanopart. Res.*, 2023, **25**, 115.

7 F. Mousavi, D. Elhamifar and S. Kargar, Copper/IL-containing magnetic nanoporous MCM-41: a powerful and highly stable nanocatalyst, *Surf. Interfaces*, 2021, **25**, 101225.

8 A. N. Chishti, Z. Ma, Y. Liu, M. Chen, J. Gautam, F. Guo, L. Ni and G. Diao, Synthesis of highly efficient and magnetically separable Fe_3O_4@C-TiO_2-Ag catalyst for the reduction of organic dyes and 4-nitrophenol, *Colloids Surf., A*, 2021, **631**, 127694.

9 J. Song, N. Ma, W. Chen, J. Chen and Q. Dai, Insights into mechanism of catalytic ozonation of cinnamyl alcohol over core–shell Fe_3O_4@SiO_2@La_2O_3 catalyst, *Sep. Purif. Technol.*, 2022, **282**, 119969.

10 M. Gong, X.-Y. Wang, M.-Q. Li, W.-X. Mu, Y.-D. Cao, H. Liu, Y.-G. Lv, X.-H. Qi and G.-G. Gao, High-efficient and recoverable $Mo_{72}V_{30}$@Fe_3O_4/C catalyst for oxidation of hydroxyfurfural, *Fuel*, 2023, **332**, 126050.

11 H. Kargar, M. Ghahramaninezhad, M. N. Shahrak and S. S. Balula, An Effective Magnetic Catalyst for Oxidative Desulfurization of Model and Real Fuels: Fe_3O_4/ZIF-8/TiO2, *Microporous Mesoporous Mater.*, 2021, **317**, 110992.

12 L. Yu, P. Pan, Y. Zhang, Y. Zhang, L. Wan, X. Cheng and Y. Deng, Nonsacrificial self-template synthesis of colloidal magnetic yolk–shell mesoporous organosilicas for efficient oil/water interface catalysis, *Small*, 2019, **15**, 1805465.

13 Q. Yue, J. Li, Y. Zhang, X. Cheng, X. Chen, P. Pan, J. Su, A. A. Elzatahry, A. Alghamdi and Y. Deng, Plasmolysis-inspired nanoengineering of functional yolk–shell microspheres with magnetic core and mesoporous silica shell, *J. Am. Chem. Soc.*, 2017, **139**, 15486–15493.

14 M. Wang, Y. Ni and A. Liu, Fe_3O_4@resorcinol–formaldehyde resin/Cu_2O composite microstructures: solution-phase construction, magnetic performance, and applications in antibacterial and catalytic fields, *ACS Omega*, 2017, **2**, 1505–1512.

15 C. Shi, C. Lin, X. Huang, Q. Wu, H. Ge and Y. Yang, Facile synthesis of magnetic resorcinol–formaldehyde resin Fe_3O_4@RF-Au composites for enhanced tetracycline photodegradation with simultaneous H_2O_2 production, *J. Mater. Sci.: Mater. Electron.*, 2024, **35**, 1–12.

16 Y. Zhao, C. Wang, S. Wang, C. Wang, Y. Liu, A. A. Al-Khalaf, W. N. Hozzein, L. Duan, W. Li and D. Zhao, Magnetic mesoporous TiO_2 microspheres for sustainable arsenate removal from acidic environments, *Inorg. Chem. Front.*, 2018, **5**, 2132–2139.

17 M. Nikoorazm, A. Ghorbani-Choghamarani and N. Noori, Oxo-vanadium(IV) Schiff base complex supported on modified MCM-41: a reusable and efficient catalyst for the oxidation of sulfides and oxidative S–S coupling of thiols, *Appl. Organomet. Chem.*, 2015, **29**, 328–333.

18 N. Amirmahani, N. O. Mahmoodi, M. Malakootian, A. Pardakhty and N. Seyedi, Pd nanoparticles supported on Fe_3O_4@SiO_2-Schiff base as an efficient magnetically

Open Access Article. Published on 20 January 2025. Downloaded on 2/7/2026 7:36:55 PM. This article is licensed under a Creative Commons Attribution-NonCommercial 3.0 Unported Licence.

recoverable nanocatalyst for Suzuki–Miyaura coupling reaction, *Res. Chem. Intermed.*, 2020, **46**, 4595–4609.

19 V. K. Juyal, A. Pathak, M. Panwar, S. C. Thakuri, O. Prakash, A. Agrwal and V. Nand, Schiff base metal complexes as a versatile catalyst: a review, *J. Organomet. Chem.*, 2023, 122825.

20 A. El-Sonbati, W. Mahmoud, G. G. Mohamed, M. Diab, S. M. Morgan and S. Abbas, Synthesis, characterization of Schiff base metal complexes and their biological investigation, *Appl. Organomet. Chem.*, 2019, **33**, e5048.

21 G.-l. Liu, S.-f. He, S. Zhang and H. Li, In situ ligand and complex transformation of an iron(III) Schiff base complex: structural evidence and theoretical calculations, *Dalton Trans.*, 2012, **41**, 6256–6262.

22 L. Pogány, B. Brachňaková, P. Masárová, J. Moncol, J. Pavlik, M. Gál, M. Mazúr, R. Herchel, I. Nemec and I. Šalitroš, Impact of the Schiff base ligand substituents on the solid state and solution properties of eleven iron(III) complexes, *New J. Chem.*, 2019, **43**, 13916–13928.

23 D. Elhamifar, D. Elhamifar and F. Shojaeipoor, Synthesis, characterization and catalytic application of a novel polyethylene-supported Fe/ionic liquid complex, *J. Mol. Catal. A: Chem.*, 2017, **426**, 198–204.

24 R. Mirbagheri and D. Elhamifar, Magnetic ethyl-based organosilica supported Schiff-base/indium: a very efficient and highly durable nanocatalyst, *J. Alloys Compd.*, 2019, **790**, 783–791.

25 D. Elhamifar, P. Mofatehnia and M. Faal, Magnetic nanoparticles supported Schiff-base/copper complex: an efficient nanocatalyst for preparation of biologically active 3,4-dihydropyrimidinones, *J. Colloid Interface Sci.*, 2017, **504**, 268–275.

26 V. Arun, N. Sridevi, P. P. Robinson, S. Manju and K. K. M. Yusuff, Ni(II) and Ru(II) Schiff base complexes as catalysts for the reduction of benzene, *J. Mol. Catal. A: Chem.*, 2009, **304**, 191–198.

27 M. Norouzi and D. Elhamifar, Phenylene and Isatin Based Bifunctional Mesoporous Organosilica Supported Schiff-Base/Manganese Complex: An Efficient and Recoverable Nanocatalyst, *Catal. Lett.*, 2019, **149**, 619–628.

28 J. Mondal, A. Modak, M. Nandi, H. Uyama and A. Bhaumik, Triazine functionalized ordered mesoporous organosilica as a novel organocatalyst for the facile one-pot synthesis of 2-amino-4*H*-chromenes under solvent-free conditions, *RSC Adv.*, 2012, **2**, 11306–11317.

29 S. K. Kundu and A. Bhaumik, A triazine-based porous organic polymer: a novel heterogeneous basic organocatalyst for facile one-pot synthesis of 2-amino-4*H*-chromenes, *RSC Adv.*, 2015, **5**, 32730–32739.

30 A. Maleki, A. A. Jafari and S. Yousefi, Green cellulose-based nanocomposite catalyst: design and facile performance in aqueous synthesis of pyranopyrimidines and pyrazolopyranopyrimidines, *Carbohydr. Polym.*, 2017, **175**, 409–416.

31 S. Beheshti, V. Safarifard and A. Morsali, Isoreticular interpenetrated pillared-layer microporous metal-organic framework as a highly effective catalyst for three-component synthesis of pyrano[2,3-*d*]pyrimidines, *Inorg. Chem. Commun.*, 2018, **94**, 80–84.

32 T. Farahmand, S. Hashemian and A. Sheibani, Efficient one-pot synthesis of pyrano[2,3-*d*]pyrimidinone and pyrido[2,3-*d*]pyrimidine derivatives by using of Mn-ZIF-8@$ZnTiO_3$ nanocatalyst, *J. Mol. Struct.*, 2020, **1206**, 127667.

33 J. H. Bang and K. S. Suslick, Applications of ultrasound to the synthesis of nanostructured materials, *Adv. Mater.*, 2010, **22**, 1039–1059.

34 X.-B. Zhang, H.-W. Tong, S.-M. Liu, G.-P. Yong and Y.-F. Guan, An improved Stöber method towards uniform and monodisperse Fe_3O_4@C nanospheres, *J. Mater. Chem. A*, 2013, **1**, 7488–7493.

35 B. S. Heidari, V.-S. Cheraghchi, S. Motahari, G. H. Motlagh and S. M. Davachi, Optimized mercapto-modified resorcinol formaldehyde xerogel for adsorption of lead and copper ions from aqueous solutions, *J. Sol-Gel Sci. Technol.*, 2018, **88**, 236–248.

36 B. Tahmasbi and A. Ghorbani-Choghamarani, Magnetic MCM-41 nanoparticles as a support for the immobilization of a palladium organometallic catalyst and its application in C–C coupling reactions, *New J. Chem.*, 2019, **43**, 14485–14501.

37 M. Norouzi and D. Elhamifar, Phenylene and isatin based bifunctional mesoporous organosilica supported Schiff-base/manganese complex: an efficient and recoverable nanocatalyst, *Catal. Lett.*, 2019, **149**, 619–628.

38 Y. Zhang, W. Ma, D. Li, M. Yu, J. Guo and C. Wang, Benzoboroxole-Functionalized Magnetic Core/Shell Microspheres for Highly Specific Enrichment of Glycoproteins under Physiological Conditions, *Small*, 2014, **10**, 1379–1386.

39 G. Liu, D. Wang, F. Zhou and W. Liu, Electrostatic Self-Assembly of Au Nanoparticles onto Thermosensitive Magnetic Core-Shell Microgels for Thermally Tunable and Magnetically Recyclable Catalysis, *Small*, 2015, **11**, 2807–2816.

40 S. Abaeezadeh, D. Elhamifar, M. Norouzi and M. Shaker, Magnetic nanoporous MCM-41 supported ionic liquid/palladium complex: an efficient nanocatalyst with high recoverability, *Appl. Organomet. Chem.*, 2019, **33**, e4862.

41 M. M. Heravi, A. Ghods, K. Bakhtiari and F. Derikvand, Zn[(L) proline]2: an efficient catalyst for the synthesis of biologically active pyrano[2,3-*d*]pyrimidine derivatives, *Synth. Commun.*, 2010, **40**, 1927–1931.

42 G. M. Ziarani, S. Faramarzi, S. Asadi, A. Badiei, R. Bazl and M. Amanlou, Three-component synthesis of pyrano[2,3-*d*]-pyrimidine dione derivatives facilitated by sulfonic acid nanoporous silica (SBA-Pr-SO_3H) and their docking and urease inhibitory activity, *Daru, J. Pharm. Sci.*, 2013, **21**, 1–13.

43 M. Bararjanian, S. Balalaie, B. Movassag and A. Amani, One-pot synthesis of pyrano[2,3-*d*]pyrimidinone derivatives catalyzed by L-proline in aqueous media, *J. Iran. Chem. Soc.*, 2009, **6**, 436–442.

© 2025 The Author(s). Published by the Royal Society of Chemistry